Chapter 3:

Alkene epoxidation catalyzed by vanadium heteropoly acids heterogenized on amine functionalized SBA-15 materials

3.1 Introduction

Heterogenization of homogeneous catalytic materials has been an attractive strategy to overcome the difficulties involved in the separation and reusability of homogeneous catalysts [1, 2]. Many strategies have been adopted in the literature to heterogenize the homogeneous catalysts. Conventionally they are immobilized/anchored on polymeric organic materials such as resins [3, 4], supported on inert porous solids such as alumina and silica [5, 6] or encapsulated in the pores and cavities of microporous and mesoporous materials such as zeolites, MCM-41 and SBA-15 [7-9]. There are certain disadvantages with polymeric supports due to their vulnerability of their organic part to some chemicals and solvents, and due to leaching of catalysts from the immobilized material over the period of reactions [10]. On the other hand, porous inorganic material supports are structurally stable and more resistant to organic chemicals and solvents. However, mere encapsulation of the homogeneous catalytic molecules into the porous materials may also lead to partial leaching of catalysts. Moreover, controlling the amount of catalysts loading is limited when encapsulation technique is adopted [11].

To overcome the leaching problem, efforts have been made to immobilize the catalytic molecules on a functionalized silica surface, for example, microporous and mesoporous materials with organic chain containing terminal functional groups like amine, phosphine, sulfide etc [2]. Anchoring of the homogeneous catalysts onto these functionalized materials is proven to be effective in reducing the leaching problem. These inorganic materials are more versatile than polymeric supports since pore dimensions, specific surface area and mesoporous structure of them can be controlled to a large extend. A great deal of research work has been done on X and Y-type zeolites and M41 based mesoporous materials. Amongst mesoporous materials, SBA type support materials are more attractive due to their better hydrothermal stability, large pores and thick walls.

Transition metal ion substituted heteropoly compounds are, in general, promising catalysts for many catalytic applications including selective oxidation reactions [12]. High solubility of these molecules often makes their separation from the reaction mixture difficult. Heterogenizing these homogeneous molecules by immobilizing on mesoporous materials (e.g. MCM-41, SBA-15) were successful and found to be stable and active [13-16]. It was found that the encapsulation technique enhanced easy separation of these heteropoly anions from the reaction mixture,

however, weak bonding interaction of heteropoly anion with the silanol group of these silicate materials leads to partial leaching especially with polar solvent media [17, 18]. In the recent literature, anchoring of homogeneous catalyst molecules onto amine funtionalized silica materials like propyl amine functionalized mesoporous materials was found to be a promising strategy to reduce the leaching of active sites [18-20].

The present chapter describes the anchoring of vanadium substituted phosphomolybdic acids viz. $H_4PMo_{11}VO_{40}$, $H_5PMo_{10}V_2O_{40}$ and $H_6PMo_9V_3O_{40}$ on amine functionalized SBA-15 and their physicochemical characterization. Catalytic reactions towards the epoxidation of alkenes over *aq.* H_2O_2 and TBHP as the oxidants have been carried out, to demonstrate the heterogeneous nature and reusability of the immobilized catalyst. A comparative study of the activity of these three heteropoly acids in neat or anchored condition have been also been studied for the epoxidation reactions over both *aq.* H_2O_2 and TBHP as oxidants. In addition to this, we have also attempted to elucidate the plausible mechanism of the reactions for neat catalysts with our set of conditions, taking the aid of various techniques like UV-visible, ^{51}V NMR and EPR spectroscopy, as shall be seen in further sections.

3.2 Experimental

3.2.1 Materials

All chemicals used are of analytical reagent grade. Sodium phosphate dibasic dodecahydrate, sodium molybdate dihydrate and sodium metavanadate, conc. H_2SO_4 (Loba Chemicals Ltd) were used as received for the preparation of vanadium substituted phosphomolybdic acids. *Aq.* H_2O_2 (30%) and *aq.* TBHP (70%) were purchased from Merck India Ltd. Diethyl ether acetonitrile and 1,2 dichloroethane (S. D. Fine Chemicals Ltd) were of analytical grade and used without further purification. The exact strength of hydrogen peroxide was determined by redox titration with $KMnO_4$ solution. 30% TBHP/DCE was prepared by shaking appropriate volumes of 70% *aq.* TBHP and 1,2 dichloroethane in a separating funnel, and then collecting the lower dichloroethane (DCE) layer, followed by it's drying over anhydrous sodium sulfate. Tetraethyl orthosilicate (TEOS), (3-aminopropyl)-triethoxysilane (APTES), and the triblock copolymer, poly (ethylene glycol)-blockpoly (propylene glycol)-block-poly (ethylene glycol) [EO_{20}-PO_{70}-EO_{20}) were used as received (Aldrich). Hydrochloric acid (2 M) was prepared from 37% fuming hydrochloric acid (Merck).

The substrates norbornene, cyclooctene, cyclohexene and styrene were purchased from Sigma Aldrich Chemical Ltd. and were used without further purification.

3.2.2 Synthesis of SBA-15

SBA-15 was prepared by a known method as per the reported procedure [21]. In a typical procedure, 4 g of triblock copolymer, poly-(ethylene glycol)-block-poly-(propylene glycol)-block-poly (ethylene glycol) [EO_{20}-PO_{70}-EO_{20}, a template], was dispersed in 30 g distilled water and stirred for 3 h. To the resultant solution, 120 g of 2 M HCl was added under stirring and finally 8.5 g of tetraethyl orthosilicate (TEOS, a silicate precursor) was added dropwise. The resultant mixture was maintained at 40°C for 24 h under stirring and then at 110°C for 48 h under static condition in Teflon bottle. The crystallized product was filtered, washed with warm distilled water and dried at 110°C for 24 h. The dried sample was then calcined at 550°C at 1°C/min rate and holding it at 550°C for 6 h. The structure was confirmed by small angle X-ray scattering (SAXS) analysis. The surface area was determined by N_2 BET measurement at liquid nitrogen temperature. The calcined sample is referred as SBA-15 here after.

3.2.3 Preparation of amine-functionalized SBA-15

The surface modification of SBA-15 using 3-aminopropyl triethoxysilane (APTES) was carried out using a grafting method by adopting reported procedure [21]. In a typical preparation freshly activated SBA-15 (2 g) was refluxed with 50 ml of toluene (distilled over sodium and dried) to remove the occluded moisture azeotropically for 4 h. To that APTES (1 g) in 10 ml of toluene was added with stirring and refluxed for 4 h. After distilling off the solvent, the solid was filtered, washed in a soxhlet apparatus with dichloromethane, and then dried at room temperature. The product is designated as NH_2-SBA. The nitrogen elemental analysis estimated 2.3 mmol of NH_2 per gram of NH_2-SBA.

3.2.4 Preparation of vanadomolybdophosphoric acids

The three heteropoly acids of $H_4PMo_{11}VO_{40}$, $H_5PMo_{10}V_2O_{40}$ and $H_6PMo_9V_3O_{40}$ were synthesized by known procedures [22]. All the three heteropoly

acids were subjected to FT-IR and elemental analysis, to check the formation and purity of the same [13].

3.2.4.1 Monovanadomolybdophosphoric acid, $H_4PMo_{11}VO_{40}$ (V_1HPA)

Sodium phosphate dibasic dodecahydrate (1.77 gm, 5 mmol), was dissolved in 25 ml water and mixed with sodium metavanadate (1.52 gm, 12.5 mmol) that was dissolved in 25 ml boiling water. The mixture was cooled and acidified to red color with 1.25 ml concentrated sulfuric acid. To this colored solution was added sodium molybdate dihydrate (33.25 gm, 137.42 mmol) in 50 ml of water. Finally 21.25 ml of concentrated sulfuric acid was added. Color of the solution became light red. After cooling the solution was extracted with four fractions each of 25 ml diethyl ether to isolate the heteropoly acid in a separating funnel. In this extraction the heteropoly etherate was present as the middle layer. After separation, a stream of air was passed through the heteropoly etherate layer to free it of ether. The orange solid that separated was dissolved in water, concentrated to the first appearance of crystal in a vacuum desiccator over concentrated sulfuric acid and then allowed to crystallize further. The orange crystals that formed were dried, crushed and used for further studies.

3.2.4.2 Divanadomolybdophosphoric acid, $H_5PMo_{10}V_2O_{40}$ (V_2HPA)

Sodium metavanadate (4.06gm, 33.29 mmol) was dissolved by boiling in 16.6 ml water and then mixed with a solution of sodium phosphate dibasic dodecahydrate (1.18 gm, 3.29 mmol) in 16.6 ml water. To the cooled solution was added 0.83 ml of concentrated sulfuric acid. The resulting solution developed a red color. Addition of sodium molybdate dihydrate (20.16 gm, 83.32 mmol) in 50 ml water was then done. While the solution was stirred vigorously 14.16 ml of concentrated sulfuric acid was added slowly and then the hot solution was cooled to room temperature. The title compound was then extracted with four fractions each of 20 ml diethyl ether in a separating funnel. The heteropoly acid was present as the etherate in the bottom layer. This layer was isolated and dried in order to make it ether free. Orange colored solid was obtained after complete drying. Pure complex was obtained after recrystallization in water. The crystals that formed were dried and crushed for further use.

3.2.4.3 Trivanadomolybdophosphoric acid, $H_6PMo_9V_3O_{40}$ (V_3HPA)

Sodium phosphate dibasic dodecahydrate (1.77 gm, 4.95 gm) was dissolved in 12 ml water. Sodium metavanadate (9.15 gm, 75.04 mmol) was made soluble by boiling in 50 ml water. The sodium phosphate solution was mixed with the sodium metavanadate solution. The resulting solution was cooled, followed by the addition of 1.25 ml of concentrated sulfuric acid. This red colored solution was then added to a solution of sodium molybdate dihydrate (13.62 gm, 56.3 mmol) in 37.5 ml water. This solution was stirred vigorously and simultaneously 21.25 ml of concentrated sulfuric acid was added. The hot solution was cooled to ambient conditions. The heteropoly acid formed was extracted with four fractions, each of 25 ml diethyl ether in a separating funnel. The heteropoly acid is present as the etherate in the middle fraction. The middle layer was then isolated, dried to free of ether. The resulting red colored solid obtained was dissolved in water, concentrated to first crystal formation and allowed to crystallize further. The red crystals that formed were dried and powdered prior to further use.

3.2.5 Anchoring of vanadomolybdophosphoric acids onto NH_2-SBA

Freshly activated NH_2-SBA (0.9 g) was added 50 ml of acetonitrile solution containing 0.1 g of vanadomolybdophosphoric acids (V_xHPA, x: 1, 2 or 3) and refluxed for 3 h. The sample was then filtered, washed, and soxhleted using acetonitrile solvent for 12 h and dried at 100°C under vacuum. The final materials are designated as NH_2- SBA-V_xHPA (x: 1, 2 or 3). The nitrogen elemental analysis estimated 2.1 mmol of NH_2 per gram of NH_2-SBA-V_1HPA. Vanadium content estimated by ICP-OES and was 0.24 ppm for NH_2-SBA-V_1HPA.

3.2.6 Characterization

SAXS pattern of the samples was obtained in reflection mode using a Rigaku D_{max} 2500 diffractometer and Ni filtered copper radiation. The samples were scanned in the range 2θ = 0.5 - 6 and the generator was operated at 40 kV and 150 mA. Nitrogen adsorption measurements were measured on a NOVA 1200 (Quantachrome) at 77 K. First the samples were activated at 453 K for 3 h under vacuum and then the adsorption-desorption was conducted by passing N_2 into the sample, which was kept under liquid nitrogen. The specific surface area of the samples were calculated using

the multiple-point Brunauer-Emmett-Teller (BET) method in the relative pressure range P/P_0 = 0.05-0.3. The pore size distribution curves were computed by using the Barrett-Joyner-Halenda (BJH) method. The pore sizes were obtained from the peak positions of the distribution curves. Thermal analysis was performed on a Seiko model instrument (TG DTA 32) and the thermograms recorded at a heating rate of 10°C min^{-1} from 30 to 600°C under nitrogen atmosphere.

The elemental analysis (C and N) was carried out with an EA 1108 Elemental Analyser (Carlo Erba Instruments). V and Mo contents were estimated by ICP (Perkin Elmer Plasma 1000 Emission Spectrometer). The FT-IR spectra for the powdered samples were obtained over a range of 4000 - 400 cm^{-1} on a Shimadzu FT-IR 8201 PC and the spectra were recorded as a mull in fluorolube for the region 4000 - 1350 cm^{-1} and as a nujol mull for 1350 - 400 cm^{-1} range. UV-visible spectra were recorded on a Shimadzu UV-visible spectrophotometer (UV-2500 PC). High-resolution NMR studies were carried out on a Bruker DRX-500 MHz spectrometer. ^{31}P NMR chemical shifts were referenced to external phosphoric acid and ^{51}V chemical shifts were referenced to $VOCl_3$. SEM pictures of the samples were recorded on a JEOL-JSM-5200 scanning electron microscope with a resolution of 5.5 nm. Room-temperature EPR spectra were recorded on a Bruker EMX X-band spectrometer operating at 100 kHz field modulation at microwave frequency, 9.766 GHz. The microwave frequency was calibrated using a frequency counter of the microwave bridge ER 041 XGD. Bruker Simfonia and WINEPR software packages were used in the spectral simulations and to calculate hyperfine coupling constant.

3.2.7 Catalytic activity

All the reactions were carried out in a glass reactor at 60°C in acetonitrile solvent. Typically 0.01 mol of substrate and 0.01 mol of aqueous hydrogen peroxide (30%) were taken in 10 ml of solvent and the catalyst, 1 g NH_2- SBA-V_xHPA (1 g contains 5 μmol of V content) where, (x: 1, 2 or 3) was added. The reaction mixture was stirred constantly at the required temperature and was subjected to GC analysis (SPB^{TM}-5, 30m x 0.53mm, 3.0μm film thickness Supelco fused silica capillary column, N_2, FID, internal standard-chlorobenzene) periodically to monitor the conversion of the substrate and selectivity of the products. In the case of the immobilized sample, amount of catalyst containing 5 μmol of V content was taken for

the reaction. After the reactions, the immobilized catalyst was removed by careful filtration, washed several times with acetonitrile, dried in air and reused. Reactions were also carried out by adding 10 mg of neat V_xHPA as the catalyst for comparison.

3.3 Results and Discussions

3.3.1 Synthesis and Characterization

The Keggin structure of the vanadomolybdophosphoric acids was confirmed by FT-IR spectroscopy. The major FT-IR peaks were: 1060 cm^{-1} for P-O_I-Mo, 960 cm^{-1} for Mo=O_t and 807 cm^{-1} and 783 cm^{-1} for Mo-O_b-Mo, where O_I, O_t and O_b are the inner, terminal and the bridging oxygen atoms respectively, in the Keggin anionic framework [13]. The water of crystallization was determined by thermo gravimetric analysis and was found to be 19, 14 and 14 for $H_4PMo_{11}VO_{40}$, $H_5PMo_{10}V_2O_{40}$ and $H_6PMo_9V_3O_{40}$ respectively. The UV-visible spectrum of the catalysts in acetonitrile showed absorption maxima at 218 and 308 nm, which are typical for the Keggin structure. These bands are due to the ligand to metal charge transfer transitions associated with octahedrally coordinated Mo^{6+} unit [13].

Amine functionalization of SBA-15 and the subsequent immobilization of molybdovanadophosphoric acids onto the mesoporous support are shown as a schematic representation in Figure 1. Vanadium substituted heteropoly acid samples were orange to red in color and the color becomes nearly colorless during the immobilization procedure. The combined filtrate after washing and soxhleting was subjected to UV-visible analysis and did not show any characteristic bands for molybdovanadophosphoric acids, possibly indicating retention of V_xHPA in the pores of NH_2-SBA. The ICP analysis of immobilized samples supports the above observation.

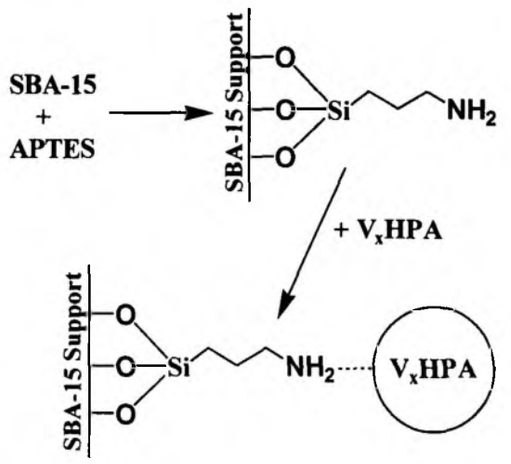

Figure 1: Schematic representation of functionalization of SBA-15 and the subsequent heterogenization of molybdovanadophosphoric acid (VHPA) on amine functionalized SBA-15

The small angle X-ray scattering (SAXS) patterns for SBA-15, NH_2-SBA and NH_2-SBA-V_xHPA (x: 1, 2 or 3) are depicted in Figure 2. Three reflections, one strong reflection at (100) and two with low intensity at (110) and (200) planes, are seen in the range 2θ = 0.9-2.0° for all the samples, indicating retention of long-range order structure and well-formed hexagonal pore arrays. The d_{100} positions are similar for all the samples that probably indicate the structural ordering of SBA-15 is not affected upon modification with APTES, and on anchoring with V_xHPA. A small reduction in intensity of reflection (100) was noticed for the immobilized samples compared to pure SBA-15 and NH_2-SBA indicating anchoring of V_xHPA has indeed occurred inside the pores of SBA-15 [20, 23].

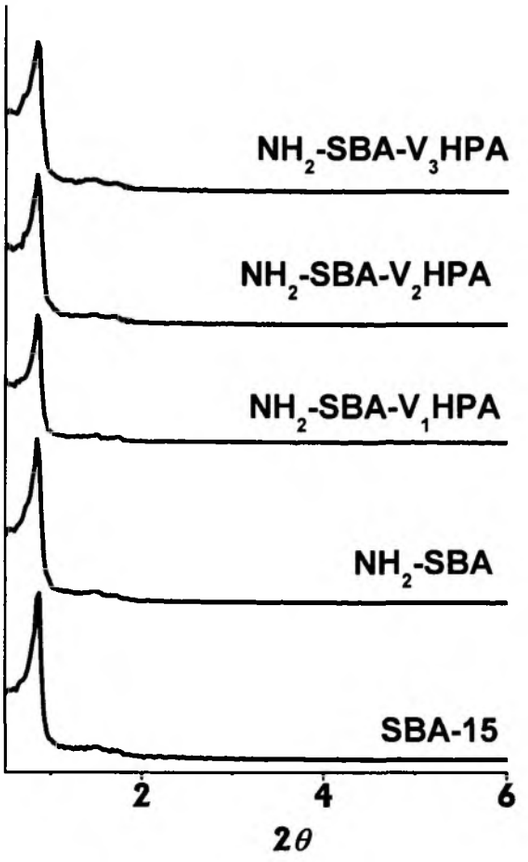

Figure 2: SAXS patterns of (a) SBA-15, (b) NH_2-SBA and (c) NH_2-SBA-V_1HPA, (d) NH_2-SBA-V_2HPA and (e) NH_2-SBA-V_3HPA

The nitrogen sorption isotherms for SBA, NH_2-SBA and NH_2-SBA-V_1HPA samples were carried out by BET method at 77 K. The parameters calculated from nitrogen adsorption data using the BJH method are listed in Table 1. The isotherm patterns of these samples display a type IV isotherm with H1 hysteresis and a sharp increase in volume adsorbed above $P/P_0 \sim 0.7$ which is characteristic of highly ordered mesoporous materials and are depicted in Figure 3. The textural properties of SBA-15 are substantially maintained over amine functionalization and on subsequent immobilization of V_1HPA. Surface area of SBA-15 has reduced from 859 m^2/g to 365 $\pm$ 15 m^2/g on amine functionalization and upon anchoring the V_xHPA [23, 24]. Similarly there was a reduction in pore volume on functionalization and on loading of V_xHPA compared with that of the pure SBA-15. These observations indirectly

confirm the anchoring of V_1HPA onto NH_2-SBA. The reduction in surface area and pore volume might be due to the filling of pores by bulkier trisiloxypropyl amine group and the heteropoly acid anions. The BJH pore size distribution curves (Figure 3, inset) derived from the desorption isotherm were similar for all the samples. The observation of similar pore size distribution for all the samples again indicates the integrity of ordered pore structure.

Table 1: Structural properties of SBA-15, NH_2-SBA and NH_2-SBA-VHPA samples characterized by N_2 adsorption

Samples	S_{BET} (m^2/g)	Total pore volume (cm^3/g)	Average pore diameter (nm)
SBA-15	859	1.10	8.9
NH_2-SBA	360	0.64	7.1
NH_2-SBA-V_1HPA	347	0.60	6.9
NH_2-SBA-V_2HPA	349	0.62	6.7
NH_2-SBA-V_3HPA	348	0.60	6.8

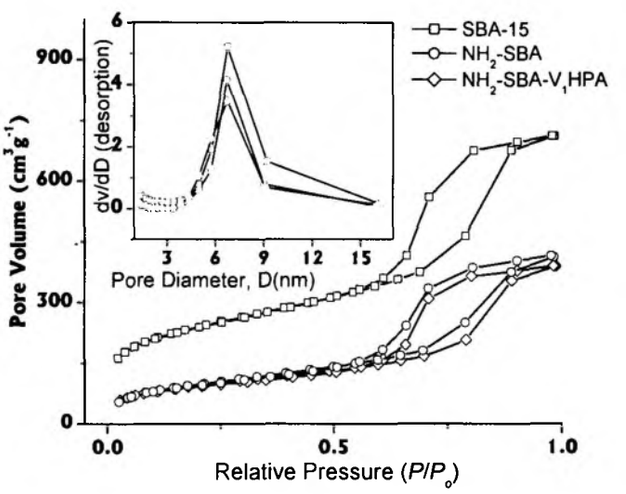

Figure 3: Nitrogen adsorption-desorption isotherms for (a) SBA-15, (b) NH_2-SBA and (c) NH_2-SBA-V_1HPA (Inset: Effective pore distribution of the above samples)

The SEM images of SBA (A), NH_2-SBA (B) and NH_2-SBA-V_1HPA samples (C) are shown in Figure 4 and the images are similar to the reported ones [25-27]. SEM images of other two vanadium loadings were also similar. The images of all the samples show hexagonal particles organized into rope-like structures, which are further agglomerated into elongated particles.

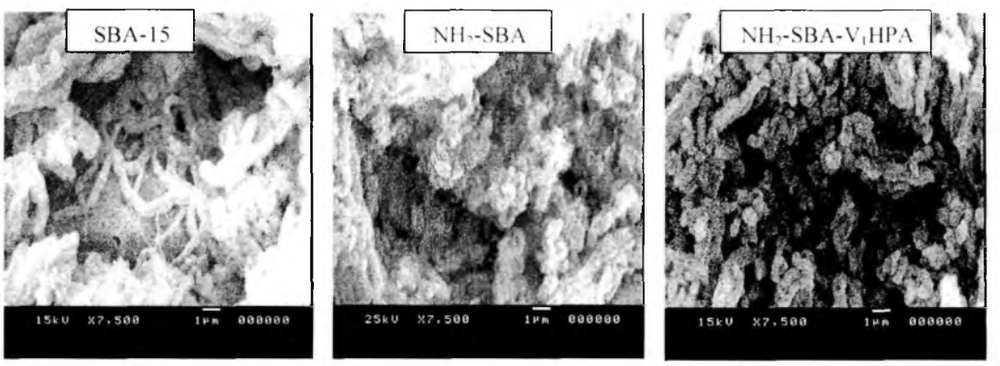

Figure 4: SEM images of (A) pure SBA-15, (B) NH_2-SBA and (C) NH_2-SBA-VHPA

3.3.2 Spectroscopic studies

Anchoring of V_1HPA on NH_2-SBA was investigated by different spectroscopic tools. The FT-IR spectra of NH_2-SBA, NH_2-SBA-V_1HPA and neat V_1HPA are compared as can be seen in Figure 5 [20]. Neat V_1HPA show peaks 1059, 958, 873, 722 cm^{-1}, characteristic of phosphomolybdic acid. Since most of the FT-IR bands of NH_2-SBA sample (1059, 958, 800 cm^{-1}) overlap with that of the neat V_1HPA, the bands associated with heteropoly unit were not clearly noticed in FT-IR spectrum of NH_2-SBA-V_1HPA. However, increase in intensity of bands at 800, 958 and 1059 cm^{-1} and appearance of a new shoulder at 894 cm^{-1} in NH_2-SBA-V_1HPA with respect to that of NH_2-SBA may be considered as an indication for the presence of V_1HPA in the pores of NH_2-SBA [13].

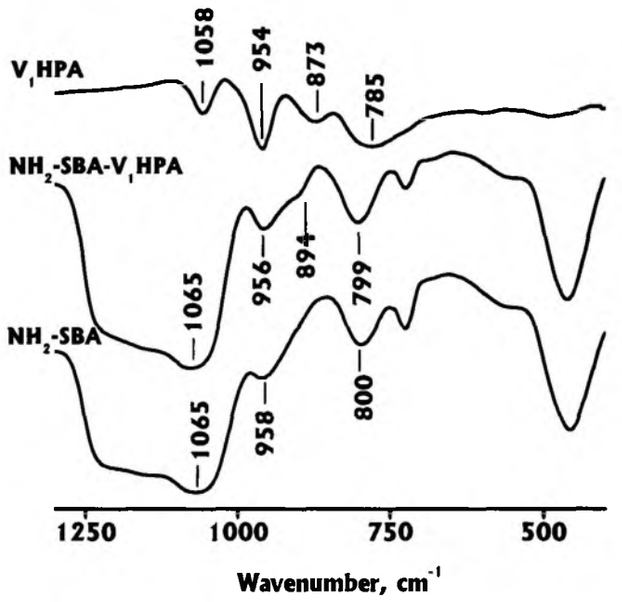

Figure 5: FT-IR spectra of (A) pure VHPA, (B) NH_2-SBA-VHPA and (C) NH_2-SBA

Similarly, V_xHPA samples show characteristic UV-visible bands and therefore their existence in SBA-15 can be identified by UV-visible spectroscopy. While SBA-15 and NH_2-SBA do not show any characteristic peaks in 220-400 nm region, NH_2-SBA-V_xHPA samples exhibit features of metal to ligand charge transfer transitions in this region as shown in Figure 6. These bands are compared with that of the neat V_1HPA (Figure 6, inset) which exhibits characteristic bands around 320 and 479 nm. Upon immobilization these bands are slightly shifted and broad features are seen at 348 and 451 nm. Some bands are shown in expanded scale for clarity. The presence of these bands indicates the occupation of V_xHPA in the pores of NH_2-SBA and small shifts in wavelength of these bands should be due to constraints around the heteropoly anion and/or due to its interaction with NH_2-SBA.

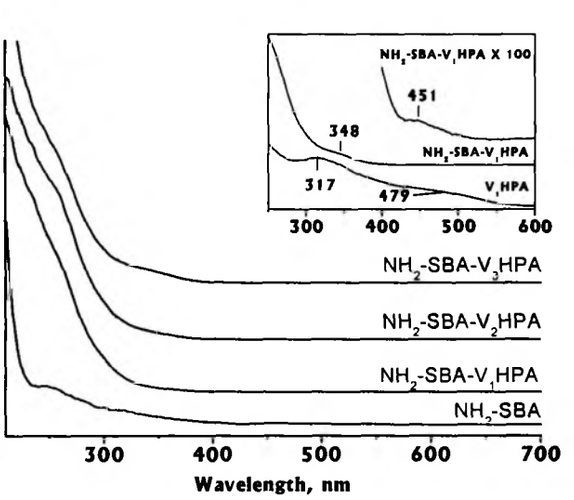

Figure 6: Diffuse reflectance UV-Visible spectra of NH_2-SBA-V_1HPA and neat V_1HPA

Additional evidence for the immobilization of V_xHPA on the amine functionalized SBA was showed by ^{31}P-NMR. ^{31}P MAS NMR spectrum was recorded for NH_2-SBA-V_1HPA as a representative sample and compared with neat V_1HPA sample in Figure 7. A ^{31}P signal was seen for the neat V_1HPA at -4.9 ppm and it was shifted to 1.85 ppm for NH_2-SBA-V_1HPA. Due to the extreme sensitivity of ^{31}P nucleus to its local environment, any slight changes in the chemical environment due to the interaction between the support and V_1HPA could have caused the difference. The difference in the chemical shift can also be due to the difference in degree of hydration of V_1HPA upon immobilization as it is known that ^{31}P NMR signal of the heteropoly acid anion is sensitive to degree of hydration [28-30]. Thus, the above spectral studies along with the small-angle X-ray and surface studies clearly provide evidence for the presence of V_xHPA inside NH_2-SBA.

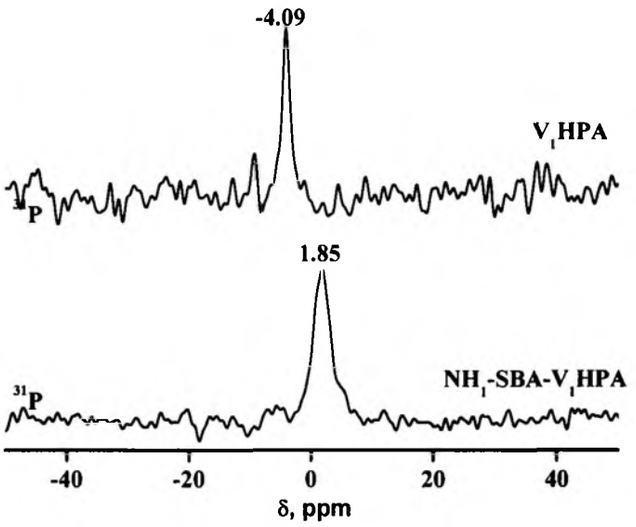

Figure 7: ^{31}P MAS NMR spectra of neat V_1HPA and NH_2-SBA-V_1HPA samples.

3.3.3 Catalytic activity and catalyst recycling

Vanadomolybdophosphoric acids are active catalysts (mostly as neat catalysts) for the selective oxidation of several organic substrates with peroxides as oxidants [31-32]. In the present work, catalytic activity of vanadomolybdophosphoric acids immobilized on the functionalized mesoporous material, NH_2-SBA-V_xHPA (x =1-3), were examined for oxygenation of cyclooctene and norbornene with oxidants in aqueous (*aq.* H_2O_2) and non-aqueous (TBHP/DCE) medium. Reactions with the neat V_xHPA (homogeneous) catalysts were also carried out with both the oxidants under the same experimental conditions and the results are compared with the respective immobilized catalysts (NH_2-SBA-V_xHPA).

In Figure 8, kinetic plots of cyclooctene conversion of the reactions with *aq.* H_2O_2 and TBHP/DCE in acetonitrile are given for V_1HPA, V_2HPA and V_3HPA catalysts. The reactions were carried out for 5 h as there after not much appreciable conversion was noticed. For V_1HPA the conversion of cyclooctene with *aq.* H_2O_2 was gradual and steady with time and reached around 42 % after 5 h of reaction time. However, with the other two catalysts the conversions were faster, especially with V_3HPA in the beginning and reached a steady state at lower conversions compared to V_1HPA. These observations suggest faster decomposition of *aq.* H_2O_2 with higher vanadium contents (as noticed by the effervescence soon after the addition of H_2O_2).

In other words, the dismutation reaction of H_2O_2 which leads to formation of O_2 and H_2O dominates the V-oxo species formation. It should be noted here that the V-oxo species is responsible for the formation of desired products.

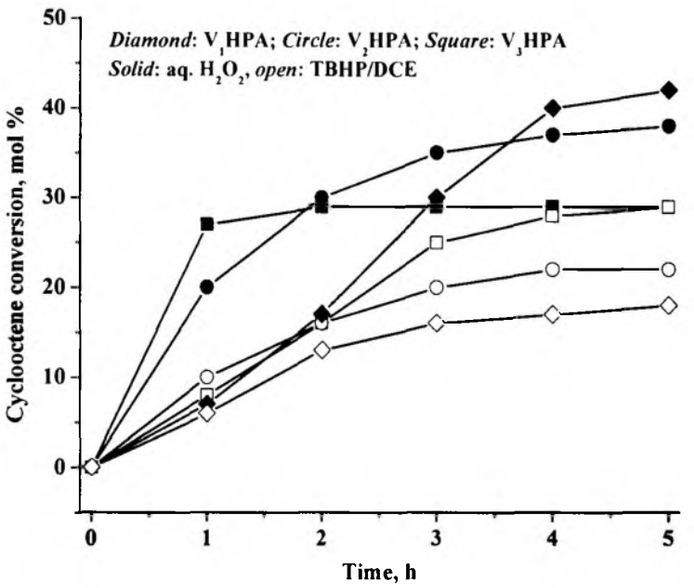

Figure 8: Reaction profiles of cyclooctene oxidation with *aq.* H_2O_2 and TBHP/DCE with the neat catalysts V_xHPA. Reaction condition: catalyst = 100 mg; cyclooctene = 0.01 mol; aqueous H_2O_2 /TBHP/DCE = 0.01 mol, 60 °C, acetonitrile

With the TBHP/DCE, the reverse trends were observed i.e. conversions are higher with higher amounts of vanadium contents though the overall conversions with TBHP/DCE were lower than that of the reactions with *aq.* H_2O_2. The lower conversion with TBHP should be due to slow decomposition of peroxides. However, here it should be noted that epoxide was only the product with TBHP/DCE but with *aq.* H_2O_2 apart from cyclooctene epoxide as a major product, other minor products such as cyclooctanol and cyclooctanone were also observed (Table 2). Formation of cyclooctanol is due to acid catalyzed reaction by protons coming from *aq.* H_2O_2 decomposition and subsequent secondary oxidation of cyclooctanol by the redox

center leads to cyclooctanone (Scheme 1). Such acid catalyzed reaction may not be possible with TBHP decomposition.

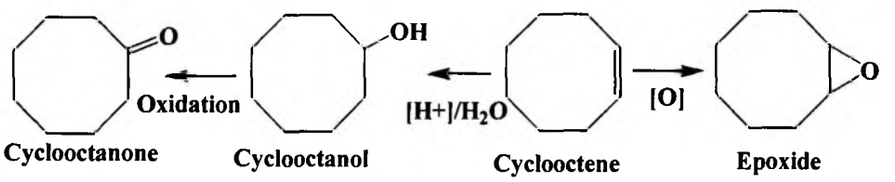

Scheme 1 Different possible products during cyclooctene oxidation reaction catalyzed by $H_4[PMo_{11}VO_{40}]$ in the presence of *aq.* H_2O_2

The above reactions were also tested with the heterogenized catalysts (NH_2-SBA-V_xHPA) with *aq.* H_2O_2 and TBHP/DCE in acetonitrile solvent. The reactions with TBHP/DCE were found to be slow due to slow decomposition of TBHP and so they were monitored for 12 h while reactions with *aq.* H_2O_2 were monitored for 5 h. The results (Table 2) show that epoxide was the only product for the both the oxidants. It may be noted here that the products were non-selective with the neat catalysts when *aq.* H_2O_2 was used. Absence of alcohol or ketone formation with the immobilized catalysts might be due to the non-availability of protons (which are responsible for alcohol formation) in the presence of NH_2-SBA. Thus epoxide was the only product.

Table 2-*A:* Oxidation of cyclooctene and norbornene with *aq.* H_2O_2 and TBHP/DCE using the neat (V_1HPA) and heterogenized (NH_2-SBA-V_1HPA) catalysts

Substrate	Oxidant	V_1HPA		NH_2-SBA-V_1HPA	
		% Conv.	Products (% Selectivity)	% Conv.	Products (% Selectivity)
Cyclooctene	H_2O_2	42	Epoxide(75)	21	Epoxide (>99)
			Cyclooctanol (13)		
			Cyclooctanone (12)		
	TBHP	18	Epoxide (>99)	34	Epoxide (>99)
				32*	Epoxide (>99)*
Norbornene	H_2O_2	70	Epoxide (58)	50	Epoxide (>99)
			Norborneol(17)		
			Norbornanone(25)		
	TBHP	32	Epoxide (>99)	40	Epoxide (>99)
				38*	Epoxide (>99)*

Reaction conditions: V_1HPA catalyst: 5 μM, NH_2-SBA-V_1HPA (corresponding to 5 μM of heteropoly anion): 100 mg, substrate: 0.01 mol, *aq.* H_2O_2: 0.01 mol, TBHP/DCE: 0.01 mol, acetonitrile (10 ml), 60°C, time: 5 h (Reaction time with TBHP/DCE: 12 h), *: recovered catalyst (second run)

Table 2-*B:* Oxidation of cyclooctene and norbornene with *aq.* H_2O_2 and TBHP/DCE using the neat (V_2HPA) and heterogenized (NH_2-SBA-V_2HPA) catalysts

Substrate	Oxidant	V_1HPA		NH_2-SBA-V_1HPA	
		% Conv.	Products (% Selectivity)	% Conv.	Products (% Selectivity)
Cyclooctene	H_2O_2	38	Epoxide(70)	25	Epoxide (>99)
			Cyclooctanol (18)		
			Cyclooctanone (12)		
	TBHP	22	Epoxide (>99)	26	Epoxide (>99)
				25*	Epoxide (>99)*
Norbornene	H_2O_2	51	Epoxide (55)	32	Epoxide (>99)
			Norborneol(20)		
			Norbornanone(25)		
	TBHP	26	Epoxide (>99)	30	Epoxide (>99)
				28*	Epoxide (>99)*

Reaction conditions: V_2HPA catalyst: 5 μM, NH_2-SBA-V_2HPA (corresponding to 5 μM of heteropoly anion): 100 mg, substrate: 0.01 mol, *aq.* H_2O_2: 0.01 mol, TBHP/DCE: 0.01 mol, acetonitrile (10 ml), 60°C, time: 5 h (Reaction time with TBHP/DCE: 12 h), *: recovered catalyst (second run)

Table 2-*C*: Oxidation of cyclooctene and norbornene with *aq.* H_2O_2 and TBHP/DCE using the neat (V_3HPA) and heterogenized (NH_2-SBA-V_3HPA) catalysts

Substrate	Oxidant	V_1HPA		NH_2-SBA-V_1HPA	
		% Conv.	Products (% Selectivity)	% Conv.	Products (% Selectivity)
Cyclooctene	H_2O_2	29	Epoxide(60)	22	Epoxide (>99)
			Cyclooctanol (22)		
			Cyclooctanone (18)		
	TBHP	29	Epoxide (>99)	24	Epoxide (>99)
				22*	Epoxide (>99)*
Norbornene	H_2O_2	45	Epoxide (55)	30	Epoxide (>99)
			Norborneol(22)		
			Norbornanone(23)		
	TBHP	21	Epoxide (>99)	29	Epoxide (>99)
				27*	Epoxide (>99)*

Reaction conditions: V_3HPA catalyst: 5 μM, NH_2-SBA-V_3HPA (corresponding to 5 μM of heteropoly anion): 100 mg, substrate: 0.01 mol, *aq.* H_2O_2: 0.01 mol, TBHP/DCE: 0.01 mol, acetonitrile (10 ml), 60°C, time: 5 h (Reaction time with TBHP/DCE: 12 h), *: recovered catalyst (second run)

To check the possibility of leaching of the active sites, the catalyst part was separated after 2 h of cyclooctene oxidation reaction with *aq.* H_2O_2 at the experimental condition and the filtrates containing reaction mixture were then allowed to continue further under the same experimental conditions. Conversions were monitored periodically and the results are plotted in Figure 9. As seen in the figure, with NH_2-SBA-V_1HPA the progress of the reaction was negligible after filtering the catalyst. The ICP analysis results indicate < 1.1 % of vanadium leaching (out of total amount of vanadium taken) into the solution when *aq.* H_2O_2 was used. Similar leaching experiments were carried out with NH_2-SBA-V_3HPA and it was found that the progress of reaction after filtering off the catalyst was almost same as that in the

presence of the NH_2-SBA-V_3HPA (Figure 9). The results simply indicate that the leaching of vanadium content was higher with the catalysts having higher vanadium loadings, however, selectivity of the product remains high i.e. cyclooctene epoxide was the only product. The reason for the high selectivity can be explained as discussed above.

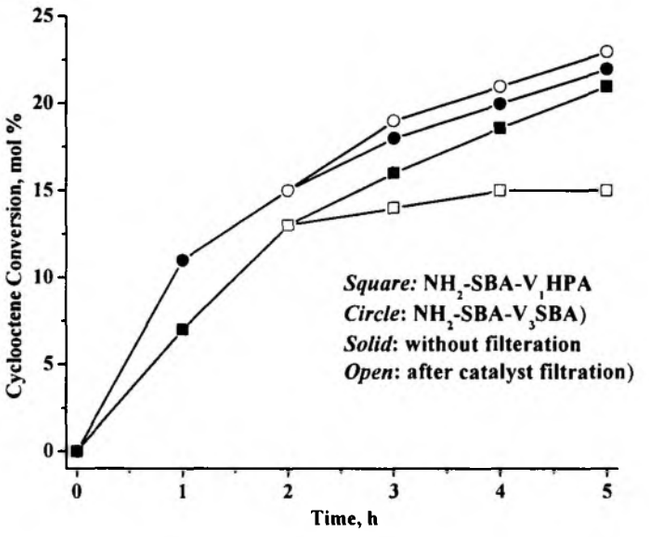

Figure 9: Reaction profiles of cyclooctene oxidation reactions with *aq.* H_2O_2 in the presence of NH2-SBA-V_1HPA and of NH_2-SBA-V_3HPA without filtration of the catalyst and after filtration of the catalyst at 2 h of reaction

Similar leaching experiments were also carried out with NH_2-SBA-V_xHPA (x: 1, 2 or 3) when TBHP/DCE oxidant was used under identical experimental condition. Slow decomposition of TBHP indicates the reactions are diffusion controlled due to the bulkiness of *t*-butyl group of TBHP. Leaching of vanadium was found to be negligible (< 0.2 % of total vanadium used) with all the three catalysts namely NH_2-SBA-V_xHPA (x: 1, 2 or 3) and the reaction results are given in Table 2. The reusability of the heterogenized catalyst was tested as follows: after 12 h of cyclooctene oxidation reaction, the NH_2-SBA-V_xHPA catalysts were filtered from the reaction mixture, washed with acetonitrile, dried in air and reused for the fresh reaction under identical experimental conditions. This cycle was repeated twice and the results are given in Table 2. It was found that with the recycled catalyst the conversion was bit low, however, selectivity remains very high.

The catalysts were also tested for oxidation of another substrate, norbornene, with the neat as well as the immobilized catalyst using both *aq.* H_2O_2 and TBHP/DCE oxidants and the results are give in Table 2. As seen in the table, with *aq.* H_2O_2 the neat catalysts always lead to multiple products formation with high conversion of substrates due the fast decomposition of H_2O_2. The formation of the minor products like norborneol and 2-norbornanone apart from the main product *i.e.* norbornene epoxide, can be explained due to the acidic nature associated with *aq.* H_2O_2 decomposition as discussed above. However, epoxide was the only product when TBHP/DCE was used. The norbornene oxidation reactions were also carried out with the anchored catalysts, NH_2-SBA-V_xHPA, with *aq.* H_2O_2 as well as TBHP/DCE oxidants and it was found that norbornene epoxide was the only product. The results are summarized in Table 2.

3.3.4 Reaction mechanism for neat V_xHPA

3.3.4.1 UV-visible spectroscopy

In our further studies, an attempt was made to propose the plausible mechanism of the reaction based on the UV-visible, ^{51}V NMR and EPR results, as seen below. Since amongst the three neat V_XHPA catalysts, V_1HPA was the most active catalyst for the epoxidation reactions, only V_1HPA was considered for the detailed mechanistic studies, over *aq.* H_2O_2 as the oxidant. For V_2HPA and V_3HPA catalysts, we expect a similar kind of mechanism.

A small amount of the reaction mixture was drawn periodically during the course of the reaction and was monitored by UV-visible spectroscopy in 200 - 900 nm region. Acetonitrile solution of the pure catalyst exhibits a characteristic band at around 308 nm (Figure 10, a) with a long tail at higher wavelength, which is associated with the ligand-metal transfer transitions. The above broad band is deconvoluted into two bands viz. a strong band at 308 nm and a weak one at 355 nm (Figure 10, dashed lines), and the line-width of both the bands are about 50 nm. Upon addition of *aq.* H_2O_2 (trace, b) or alkene + *aq.*H_2O_2 (trace, c) to the above catalyst, a distortion in the shape or line width could be noticed in the LMCT band, indicating the changes in the environment around heteropoly anion. However, the bands are not resolved enough to be noticed clearly to extract any further information. Similar was the case with the trace (d) and (e) in figure 10 corresponding to reaction mixtures at different reaction times.

V^{4+} ions with d^1 configuration are expected to show a *d-d* band around 750 nm; however, V^{5+} ions with no electron in d-orbital do not show any such a band [33-34]. A broad band around 750 nm was seen for acetonitrile solution of the pure catalyst (Figure 10, inset a) indicating that part of vanadium is in 4+ oxidation state as also evidenced by EPR spectroscopy as seen further. However, it is interesting to note that upon addition of *aq.* H_2O_2 the broad *d-d* band vanishes (Figure 10, inset b). This may indicate that the V^{4+} ions are oxidized to V^{5+} during the reaction. However, not much information could be obtained from UV-visible studies about the vanadium-peroxide interaction.

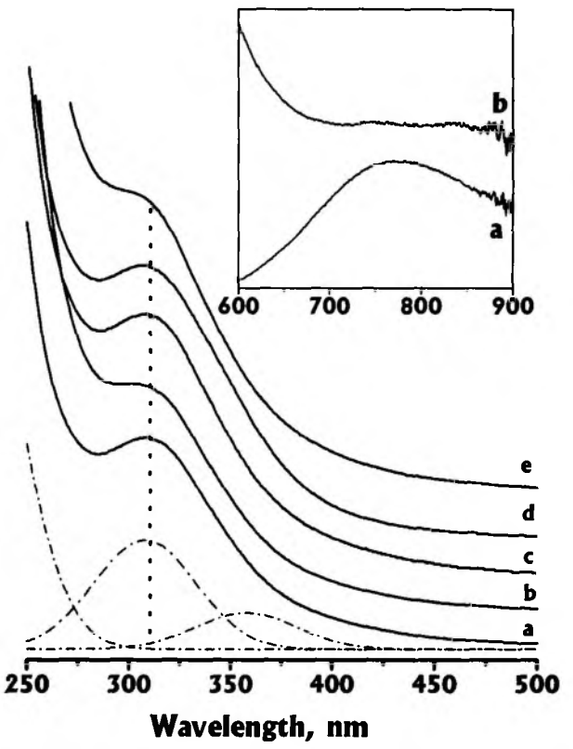

Figure 10: UV–visible spectra of LMCT region for (a)$H_4[PMo_{11}VO_{40}]$ in acetonitrile solution, (b) catalyst + *aq.* H_2O_2 in acetonitrile, (c) catalyst + norbornene in acetonitrile, reaction mixture at (d) 0.5 h and (e) 2 h (Deconvoluted bands of spectrum of (a) are given in dashed lines). (Inset: d–d band region for (a) $H_4[PMo_{11}VO_{40}]$ in acetonitrile solution, (b) $H_4[PMo_{11}VO_{40}]$ + *aq.* H_2O_2 in acetonitrile)

3.3.4.2 ^{51}V NMR spectroscopy

^{51}V NMR spectroscopy was used to gain information on the possible catalytic intermediates formed during alkene oxidation reactions. ^{51}V NMR spectra of pure $H_4[PMo_{11}VO_{40}]$ in acetonitrile solution, of $H_4[PMo_{11}VO_{40}]$ treated with *aq.* H_2O_2 (in acetonitrile) and of the reaction mixture are shown in Figure 11. The pure sample mainly shows a single peak at -540.1 ppm (Figure 11, bottom) indicating all the five isomers of $H_4[PMo_{11}VO_{40}]$ are not resolved in acetonitrile solvent [35]. There are other tiny peaks around −548 ppm most probably due to the presence of other isomers in small amount, or any vanadyl species. However, upon addition of *aq.* H_2O_2, a set of three broad signals appeared in the upfield positions at -640.8, -651.3, -671.6 ppm (Figure 11, center). This large upfield chemical shift can be attributed to $H_4[PMo_{11}VO_{40}]$-peroxo compounds as discussed in the case of hydrogen peroxide-treated $H_4[PMo_{10}V_2O_{40}]$ species in acetic acid [36], and no strong peaks were seen around -540 ppm except a small peak at -534.5 ppm. However, for the reaction mixture ($H_4[PMo_{11}VO_{40}]$ + *aq.* H_2O_2 + alkene in acetonitrile), the upfield broad bands disappeared but a narrow signal at -529 ppm (figure 11, top) was exhibited along with a peak with lower intensity at -548.1 ppm.

Disappearance of the broad upfield peaks on addition of alkenes (which is equivalent to the reaction mixture) and appearance of the narrow peak at around -548 ppm clearly indicates that the bound peroxide moiety is released from Keggin unit and the heteropoly anion unit has retained its structure after completion of the reaction. The small downfield shift of ^{51}V NMR signal for the reaction mixture compared with that of pure catalyst sample may be an indication of small structural changes like different degrees of hydration around the vanadium centers.

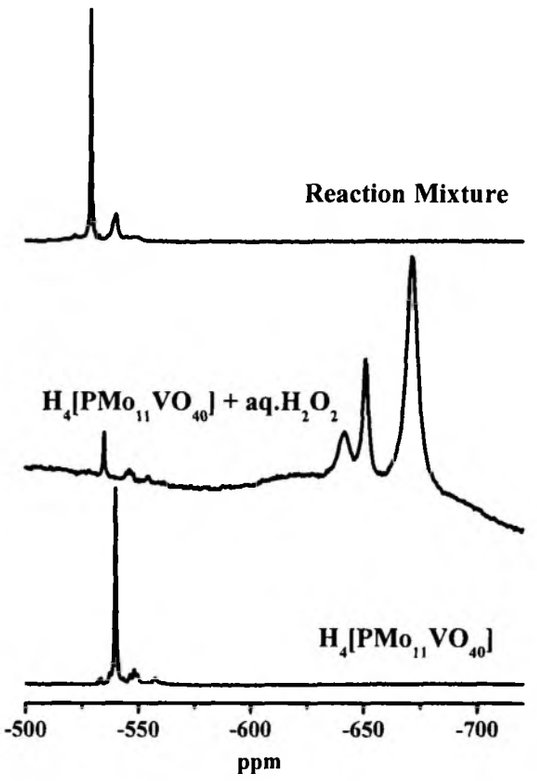

Figure 11: ^{51}V NMR spectra at room temperature for (a) $H_4[PMo_{11}VO_{40}]$ in acetonitrile solution, (b) $H_4[PMo_{11}VO_{40}]$ + *aq.* H_2O_2 in acetonitrile and (c) reaction mixture at 0.5 h

3.3.4.3 EPR spectroscopy

EPR spectroscopy can be used to monitor V^{4+} ion and any paramagnetic transient species formed during the course of the reaction. In an effort to understand the reaction intermediates and to throw light on the reaction mechanism, a small amount of sample was drawn from the reaction mixture at different time intervals and EPR spectra were recorded after the sample was quenched at room temperature. To gain a better understanding, the EPR spectra of acetonitrile solution of the catalyst before and after addition of *aq.* H_2O_2 and the substrate were also recorded. Representative spectra of such experiments are given in Figure 12. The acetonitrile solutions of the pure catalyst at room temperature exhibits isotropic ^{51}V hyperfine lines (figure 12, top) due to the presence of trace amounts of V^{4+} ion species in the catalyst or alternatively due to the vanadyl counter cations. Bayer *et al* have reported

that a small quantity of vanadium is probably present as VO^{2+} ions outside the Keggin structure compensating for two H^+ ions viz. $(VO)^{2+}H_2[PMo_{11}VO_{40}]$ during the synthesis of $H_4[PMo_{11}VO_{40}]$ [37].

The EPR spectrum contains eight hyperfine lines pattern due to the interaction of paramagnetic electron of V^{4+} with its nucleus (I = 7/2). The Hamiltonian parameters of this species based on the computer simulation are: g_{iso} = 1.97 and A_{iso} = 109 G. A small difference between the eight different lines is noticed due to the second order hyperfine effect. Addition of *aq.* H_2O_2 to the above acetonitrile solution with or without the substrate leads to the disappearance of the V^{4+} signal instantaneously (Figure 12, center). This observation probably indicates that V^{4+} center is oxidized to V^{5+}. The vanadium ions generate V^{5+}-peroxo species (Scheme 2, species II) on interaction with H_2O_2, which may partly be in equilibrium with V^{4+}-superoxo species (Scheme 2, species III) [38].

Possibility for the presence of any other species like superoxo radical bound to V^{5+} may be ruled out as its characteristic EPR signals with small hyperfine value are not observed in the present work [39]. It is noteworthy here that the EPR of the above solution was measured subsequently at various time intervals and it was found that the solution remains EPR silent even after 24 h (Figure 12, bottom).

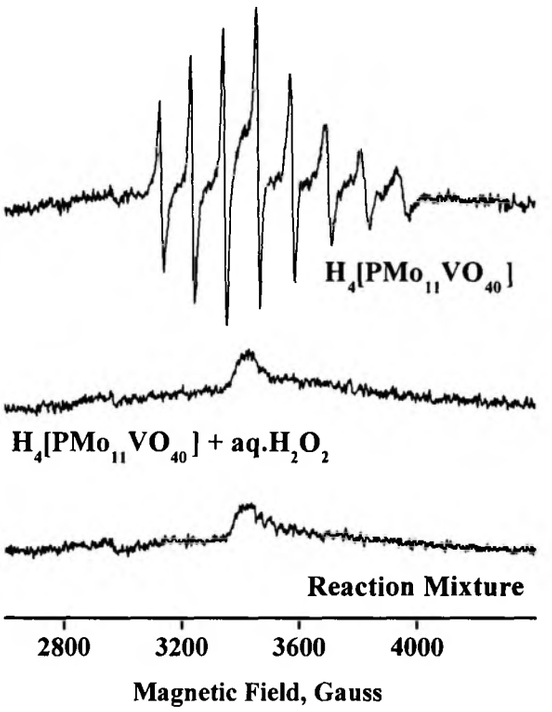

Figure 12: Room temperature EPR spectra of (a) $H_4[PMo_{11}VO_{40}]$ in acetonitrile, (b) $H_4[PMo_{11}VO_{40}]$ + *aq*. H_2O_2 in acetonitrile and (c) the reaction mixture at 0.5 h

3.3.4.4 Mechanism

Based on the catalytic studies, it is clear that the main products of norbornene or cyclooctene oxidation reaction with the V_xHPA catalyst are the corresponding epoxides and the minor products are the alcohols and ketones as can be seen in Table 2. Formation of epoxides along with hydroxylated products (alcohols) and ketones indicates that more than one mechanistic path ways are involved or subsequent reactions have proceeded after epoxide formations.

Absence of characteristic EPR signal of V^{5+}-peroxo species and appearance of upfield shift in ^{51}V NMR for the H_2O_2 interacted V_xHPA catalyst indicate that V^{5+}-peroxo (Scheme 2, species II) is the possible active intermediate species, which may partially be in equilibrium with V^{4+}-superoxo species (Scheme 2, species III). The V^{5+}-peroxo species might have formed via unstable V^{5+}-hydroxy-hydroperoxy species (Scheme 2, species I). A plausible reaction mechanism has been proposed in Scheme

2 [38]. The mechanism involves the formation of stable V^{5+}-peroxo species, as described in Scheme 2, which is partially in equilibrium with V^{4+}- superoxo radical transient species. This transient species then interacts rapidly with the alkenes to form the metallo-peroxy-alkene intermediate (Scheme 2, species IV). In the subsequent step, breakage of bonds between the oxygen atoms in this intermediate species leads to the formation of epoxides.

A mixture of corresponding alcohols and ketones are always seen as the side products in the oxidation reaction when *aq.* H_2O_2 is used as an oxidant (Table 2). The formation of hydroxylated products (alcohols) is due to the acid catalyzed hydration reaction with the alkenes (Scheme 1), where the acidity came from the protons formed upon H_2O_2 activation by the vanadium centers of the catalyst. The other minor products of ketones are formed by the oxidation of the alcohols (Scheme 1). Such acid catalyzed reaction may not be possible with TBHP decomposition. Thus, when TBHP was used as the oxidant, 100 % selectivity towards the epoxide was observed for both the alkenes, with all the three V_xHPA (x = 1, 2 or 3) catalysts (irrespective of whether used in a neat manner or in an anchored fashion) as can be seen in the Table 2.

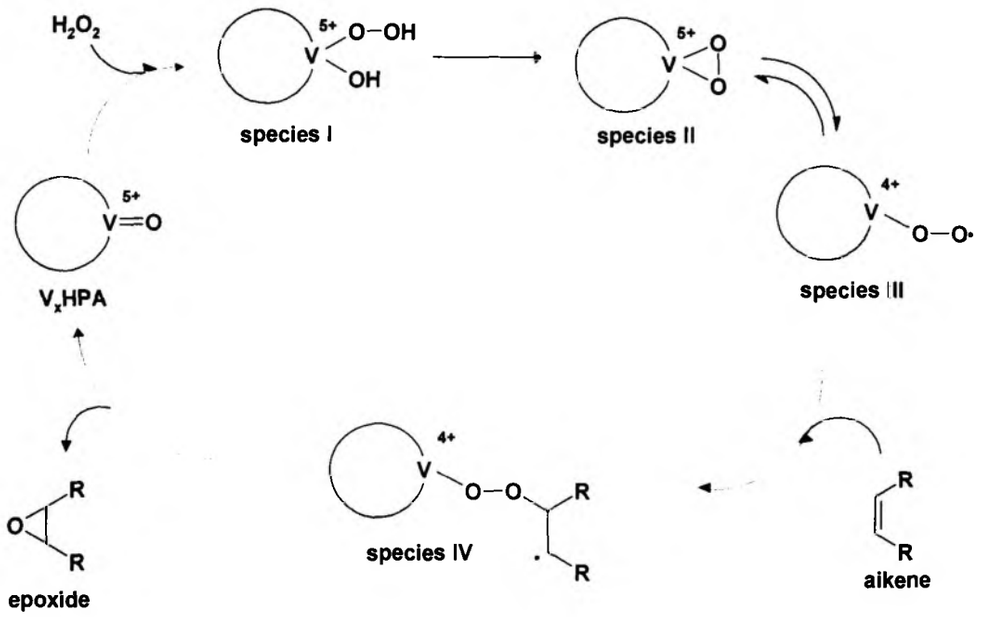

Scheme 2 A schematic representation of proposed reaction mechanism for the epoxidation of norbornene catalyzed by $H_4[PMo_{11}VO_{40}]$ in the presence of *aq.* H_2O_2. The heteropoly anion framework is represented as HPA. The bonds, which undergo changes, are alone shown for clarity

3.4 Summary and Conclusion

Vanadium substituted molybdovanadophosphoric acids (V_xHPA) were immobilized on amine functionalized SBA-15 and was characterized by different techniques. Small angle X-ray scattering analysis provides evidence for the structural integrity of the amine functionalized SBA even after immobilizing with molybdovanadophosphoric acid. The synthesized materials were also characterized by nitrogen sorption studies, UV-Visible, NMR, and IR studies provided evidence for the presence of V_xHPA inside the NH_2-SBA. The catalytic activity of the immobilized sample (NH_2-SBA-V_xHPA) were studied for few substrates with aqueous hydrogen peroxide at 60 °C and compared with the neat V_xHPA catalyst. It was found that selectivity of the products is higher with the immobilized catalyst. The catalyst part can be separated after the reaction and can be reused for few cycles without losing its further activity, especially with TBHP as the oxidant.

References:

1. G. Ertl, H. Knozinger, J. Weitkamp (Eds.), *Handbook of Heterogeneous Catalysis*, Wiley–VCH, Weinheim, 1997.
2. H. Kosslick, I. Mönnich, E. Paetzold, H. Fuhrmann, R. Fricke, D. Müller and G. Oehme, Micropor. Mesopor. Mater. 44-45 (2001) 537.
3. D. C. Bailey and S. H. Langer, Chem. Rev. 81 (1981) 109.
4. D. E. De Vos and P. A. Jacobs, Catal. Today 57 (2000) 105.
5. M. J. Naughton and R. S. Drago, J. Catal. 155 (1995) 383.
6. J. P. Arhancet, M. E. Davis, J. S. Merola and B. E. Hanson, Nature 339 (1989) 454.
7. G. A. Ozin and C. Gil, Chem. Rev. 89 (1989) 1749.
8. R. Grommen, P. Manikandan, Y. Gao, T. Shane, J. J. Shane, R. A. Schoonheydt, B. M. Weckhuysen and D. Goldfarb, J. Am. Chem. Soc. 122 (2000) 11488.
9. E. Byambajav and Y. Ohtsuka, Appl. Catal. A: General 252 (2003) 193.
10. E. Brulé and Y. R. de Miguel, Tetrahedron Lett. 43 (2002) 8555.
11. L. C. Passoni, F. J. Luna, M. Wallau, R. Buffon and U. Schuchardt, J. Mol. Catal. A: Chemical 134 (1998) 229.
12. (a) A. M. Khenkin, R. Neumann, A. B. Sorokin and A. Tuel, Catal. Lett. 63 (1999) 189; (b) B. J. S. Johnson and A. Stein, Inorg. Chem. 40 (2001) 801.
13. K. Nowińska, R. Fórmaniak, W. Kaleta and A. Wąclaw, Appl. Catal. A. 256 (2003) 115.
14. X. -B. Lu, H. Wang and R. He, J. Mol. Catal. A: Chemical 186 (2002) 33.
15. A. Ghosh, C. R. Patra, P. Mukherjee, M. Sastry and R. Kumar, Micropor. Mesopor. Mater. 58 (2003) 201.
16. W. Kaleta and K. Nowińska, Chem. Commun. (2001) 535.
17. M. J. Verhoef, P. J. Kooyman, J. A. Peters, H. van Bekkum, Micropor. Mesopor. Mater. 27 (1999) 365.
18. K. Nowińska, W. Kaleta, Appl. Catal. A. Gen. 203 (2000) 91.
19. S. Zheng, L. Gao and J. Guo, J. Solid State Chem. 152 (2000) 447.
20. J. Horniakova, T. Raja, Y. Kubota, Y. Sugi, J. Mol. Catal. A. Chemical 217 (2004) 73.
21. P. Sutra, D. Brunel, Chem. Commun. (1996) 2485.
22. G. A. Tsigdinos and C. J. Hallada, Inorg. Chem. 7 (1968) 437.
23. A. S. M. Chong, X. S. Zhao, J. Phys. Chem. B., 107 (2003) 12650.

24. S. J. Gregg, K. S. W. Singh, Adsorption, surface area and porosity, 2nd Ed,; Academic Press, London, 1982.
25. A. Lapkin, B. Bozkaya, T. Mays, L. Borello, K. Edler, B. Crittenden, Catal. Today, 81 (2003) 611.
26. D. Zhao, J. Feng, Q. Huo, N. Melosh, G. H. Fredrickson, B. F. Chmelka, G. D. Stucky, Science 279 (1998) 548.
27. M. -C. Chao, H. -P. Lin, H. -S. Sheu, C. -Y. Mou, Stud. Surf. Sci. Catal. 141 (2002) 387.
28. A. G. Siahkali, A. Philippou, J. Dwyer, M. W. Anderson, Appl. Catal. A: General 192 (2000) 57.
29. Y. Kanda, K.Y. Lee, S. Nakata, S. Asaoka, M. Misono. Chem. Lett. 1 (1988) 139.
30. V. M. Mastikhin, S. M. Kulikov, A. V. Nosov, I. V. Kozhevnikov, I. L. Mudrakovsky, M. N. Timofeeva. J. Mol. Catal. 60 (1990) 65.
31. R. Neumann, M. Cohan, Angew. Chem. Int. Ed. Engl. 36 (1997) 1738.
32. K. Nomiya, K. Yagishita, Y. Nemoto, T. -A. Kamataki, J. Mol. Catal. A. Chemical 126 (1997) 43.
33. A.M. Khenkin, A. Rosenberger, R. Neumann, J. Catal. 182 (1999) 82
34. M. Kaliva, T. Giannadaki, A. Salifoglou, C.P. Raptopoulou, A. Terzis, V. Tangoulis, Inorg. Chem. 40 (2001) 3711
35. S.E. O'Donnell, M.T. Pope, J. Chem. Soc., Dalton Trans. (1976) 2290
36. R. Neumann, M. de la Vega, J. Mol. Catal, 84 (1993) 93
37. R. Bayer, C. Marchal, F. X. Liu, A. Teze, G. Herve, J. Mol. Catal. A, 110 (1996) 65
38. H. Mimoun, L. Saussine, E. Daire, M. Postel, J. Fischer, R. Weiss, J. Am. Chem. Soc. 105 (1983) 3101
39. A.E. Gekhman, I.P. Stolarov, N.I. Moiseeva, V.L. Rubaijlo, M.N. Vargaftik, I.I. Moiseev, Inorg. Chim. Acta 275–276 (1998) 453